



CHALMERS
UNIVERSITY OF TECHNOLOGY

Design and characterization of novel graphene-enhanced vapor chambers for lightweight and high-performance electronics cooling

Downloaded from: <https://research.chalmers.se>, 2025-01-20 03:36 UTC

Citation for the original published paper (version of record):

Enmark, M., Murugesan, M., Zhang, H. et al (2025). Design and characterization of novel graphene-enhanced vapor chambers for lightweight and high-performance electronics cooling. *Nanotechnology*, 36(10).
<http://dx.doi.org/10.1088/1361-6528/ad9f6d>

N.B. When citing this work, cite the original published paper.

PAPER • OPEN ACCESS

Design and characterization of novel graphene-enhanced vapor chambers for lightweight and high-performance electronics cooling

To cite this article: Markus Enmark *et al* 2025 *Nanotechnology* **36** 105701

View the [article online](#) for updates and enhancements.

You may also like

- [Understanding the competing growth of 2D and 3D transition metal dichalcogenides in a chemical vapor deposition \(CVD\) reactor](#)
Farman Ullah, Sina Kazemian and Giovanni Fanchini
- [Quantum dots synthesis within ternary III–V nanowire towards light emitters in quantum photonic circuits: a review](#)
Giorgos Boras, Haotian Zeng, Jae-Seong Park *et al.*
- [Carbyne as a promising material for E-nose applications with machine learning](#)
Alexey Kucherik, Ashok Kumar, Abramov Andrey *et al.*



UNITED THROUGH SCIENCE & TECHNOLOGY

 **The Electrochemical Society**
Advancing solid state & electrochemical science & technology

**248th
ECS Meeting**
Chicago, IL
October 12-16, 2025
Hilton Chicago

**Science +
Technology +
YOU!**

**SUBMIT
ABSTRACTS by
March 28, 2025**

SUBMIT NOW

Design and characterization of novel graphene-enhanced vapor chambers for lightweight and high-performance electronics cooling

Markus Enmark¹ , Murali Murugesan², Hongfeng Zhang², Torbjörn M J Nilsson³, Kai J Kallio⁴, Arian Kamal⁴  and Johan Liu^{1,*} 

¹ Electronics Materials and Systems Laboratory, Department of Microtechnology and Nanoscience (MC2), Chalmers University of Technology, Kemivägen 9, SE-412 96 Göteborg, Sweden

² SHT Smart High-Tech AB, Arendals Allé 3, SE-418 79 Göteborg, Sweden

³ Saab AB, Solhusgatan 10, SE-412 76 Göteborg, Sweden

⁴ Volvo Car Corporation, Material Centre, Volvo Jakobs väg, SE-418 78 Göteborg, Sweden

E-mail: johan.liu@chalmers.se

Received 17 July 2024, revised 2 December 2024

Accepted for publication 16 December 2024

Published 6 January 2025



CrossMark

Abstract

The trend towards miniaturization of electronics and increasing transistor density in semiconductors requires more efficient cooling solutions. Vapor chambers are well established passive cooling devices that are used in a wide variety of electronics. Commercial vapor chambers are often made of high-density metals such as copper which can be a downside in lightweight applications such as laptops, smartphones, and tablets. In this study, different novel lightweight graphene-enhanced vapor chambers were built using graphene-assembled film with high thermal conductivity as envelope material. The thermal performance of the designed graphene-enhanced vapor chambers was characterized in a customized test rig and compared to a copper vapor chamber. One of the graphene-enhanced vapor chambers was shown to have 21.6% lower thermal resistance than that of a copper vapor chamber with the same design. A mass-based thermal resistance parameter was introduced as a figure of merit to account for the superior low density of the graphene-enhanced vapor chambers. The mass-based thermal resistance of the graphene-enhanced vapor chamber was seen to be 46.5% lower than that of the copper vapor chamber. The result of this study shows that replacing copper with graphene-assembled film as envelope in vapor chambers can both reduce thermal resistance and decrease the mass of the device. Hence, it is believed that graphene-enhanced vapor chambers have great potential for replacing conventional metal-based vapor chambers in lightweight and high-performance electronics and power module cooling applications in the future.

* Author to whom any correspondence should be addressed.



Original content from this work may be used under the terms of the [Creative Commons Attribution 4.0 licence](https://creativecommons.org/licenses/by/4.0/). Any further distribution of this work must maintain attribution to the author(s) and the title of the work, journal citation and DOI.

Keywords: thermal management, electronics cooling, lightweight, graphene-enhanced vapor chamber, graphene-assembled film

1. Introduction

The electronics sector has seen a continuous and predictable increase in computational power during the last 60 years. This increase has been possible due to technological improvements that have enabled more transistors to be packed into semiconductor chips. When the transistor density of a chip increases, so does the power density.

High-power density chips in modern electronics often require heavy and energy intensive thermal management systems. Small handheld electronic devices like laptops, smartphones and tablets need to be lightweight and have limited space for active cooling devices like fans and pumps [1]. One way to improve efficiency of thermal management systems without adding energy and space demanding components is by integration of passive two-phase cooling devices for heat spreading [2].

Heat pipes and vapor chambers are examples of cooling devices that make use of phase change technology of a working fluid to effectively transport heat away from a hot spot. They generally consist of three different regions: evaporator, condenser, and adiabatic region. The evaporator is placed in close vicinity to a hot spot. The liquid inside the chamber evaporates where heat is supplied and then spreads via the adiabatic region to the condenser region. After condensation, the fluid is transported back to the evaporator section via capillary forces in a wick. The wick and the working fluid are encapsulated in a sealed chamber often referred to as the envelope. The difference between a heat pipe and a vapor chamber is that the vapor chamber transports heat in two dimensions while the heat pipe only operates in one dimension. Two-phase cooling devices are today primarily made of high thermal conductivity metals such as copper or aluminum [3].

A lot of research today is focused on improving the thermal performance of heat pipes and vapor chambers by using different nanomaterials or nano structuring. It is common to target the working fluid and introduce nanoparticles to enhance thermal conductivity of the fluid [4–8]. Many studies also focus on developing nanostructured wicks to improve liquid transport of working fluids inside the vapor chamber [9–14]. However, it is uncommon to target the envelope for nanomaterial design improvements. Liu *et al* are, to the best of our knowledge, the only ones that have published a study where graphene-assembled film was used to fabricate the envelope of a heat pipe. They showed that the heat dissipation capacity per unit mass of a heat pipe with graphene envelope was 3.5 times higher than for a conventional copper heat pipe [15]. This means that using graphene-assembled film can help reduce the weight of a heat pipe while maintaining high thermal performance.

The thermal management potential of two-phase cooling devices could be improved even further if graphene-assembled film also can be used in vapor chambers. With a higher heat

dissipation capability, this graphene-based cooling technology can possibly be applied to more high-power density applications like CPUs and GPUs in future AI systems.

As the envelope constitutes most of the mass of heat pipes and vapor chambers, replacing the entire metal-based envelope with a low-density material arguably gives the most contribution to weight reduction of the device. Furthermore, copper is a finite resource which is energy intensive to produce [16]. Graphene oxide (GO), which is the precursor used in graphene-assembled films [17], can be produced from renewable sources [18] and possibly with an improved eco-friendly Hummer's method [19]. When disposed of, graphene-assembled film can easily be incinerated for energy recovery. Therefore, it can be beneficial also from a sustainability perspective to replace copper with a graphene-based material. Graphene-assembled film can be produced at a cost of around 30–50 dollars m^{-2} which is a competitive material price when compared to copper sheets of same thickness. To our knowledge, graphene-assembled films have up until now never been studied to be used as encapsulating material in vapor chambers.

In this study, lightweight and high thermal conductivity graphene-assembled films were assessed to be used as encapsulating material in vapor chambers. Important material properties for vapor chamber applications such as permeability, burst pressure and wettability were studied. Subsequently, the graphene-assembled film was used to build graphene-enhanced vapor chambers. Two different design approaches have been applied and the vapor chambers were analyzed in terms of thermal resistance. A copper vapor chamber was built using a gasket sealing technique and was compared to a graphene-enhanced vapor chamber with the same design. The characterization was done by measuring the temperature difference over the devices in a custom-made test setup that simulates a hot spot.

2. Materials and methods

2.1. Production of graphene-assembled film

The graphene-assembled film used in this study was produced with the method reported by Chen *et al* [20]. The process makes use of a scalable modified Hummer's method to exfoliate GO from graphite. The GO suspension obtained from the exfoliation step is homogenized by high shear mixing and centrifugation. Subsequently, the GO suspension is vacuum filtrated to form a GO film. The GO film is then post-processed by high temperature annealing at 2850 °C to remove oxides and a mechanical pressing step at 300 MPa to remove interlayer voids. The resulting graphene-assembled film has high thermal conductivity and flexibility. Previously, thermal conductivities up to 3826 W mK^{-1} have been measured on

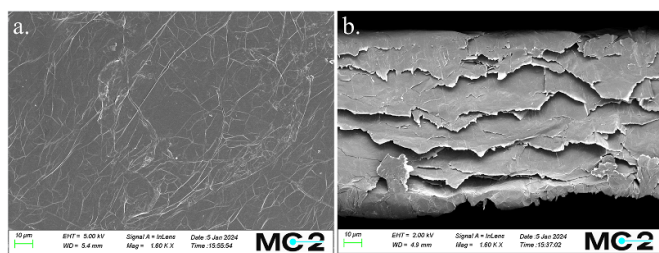


Figure 1. SEM pictures of graphene-assembled film. (a) Top view of graphene-assembled film. (b) Cross-section view of graphene-assembled film.

1 μm thick films that were produced with this method [21]. Scanning electron microscopy (SEM) pictures of a 100 μm thick graphene-assembled film seen from above and in cross-section are shown figure 1.

2.2. Evaluation of graphene-assembled film for vapor chamber applications

Graphene-assembled film needs to fulfill certain requirements to be a valid replacement to copper as encapsulating material in vapor chambers. It should be impermeable to the working fluid, it needs to withstand the potential pressure variations during operation, and the working fluid should have good wettability on the surface.

A modified Albert-Thwing cup method was used to evaluate the permeability of working fluid through graphene-assembled film. The modified Albert-Thwing cup method makes use of gas chromatography instead of gravimetry to measure the total hydrocarbon content (THC) of the analyzed gas with a flame ionization detector (FID). The improved design of the Albert-Thwing cup eliminates the effect of ethanol mass-loss through the sealing. Consequently, only the permeation of ethanol through the graphene-assembled film is measured and accounted for [22].

Figure 2 illustrates how a graphene-assembled film is assembled between two cups. During characterization, air flows through the top cup with a constant flow rate of 3 l min^{-1} and the bottom cup is filled with ethanol. The ethanol that permeates the film is detected by an FID which is connected to the air outlet. The FID used in this work was of the brand MEXA-1170HFID and was calibrated with propane gas (Air Liquide Propane N35). This means that the THC measured by the FID is given in propane equivalents. The effective carbon number method can be applied to calculate the corresponding concentration of ethanol in the analyzed air [23].

A 200 μm thick film was assembled in the modified Albert-Thwing cup as shown in figure 2. The bottom container was filled with ethanol and the sample was first conditioned at room temperature for a period of 2 months. The sample was then put in an oven to be further conditioned for 2 years and 4 months at $50\text{ }^\circ\text{C}$. During conditioning, air was continuously flowing through the top container to avoid a possible ethanol concentration increase. The ethanol in the bottom cup was replaced regularly to prevent dry-out and assure constant

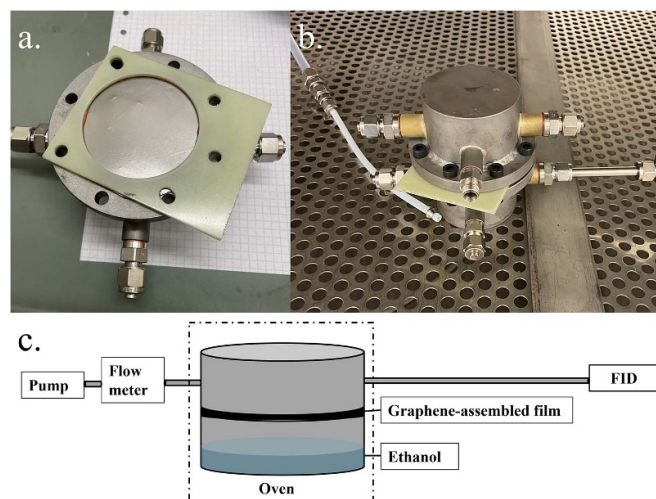


Figure 2. Test setup for measuring permeability of graphene-assembled film. (a) Graphene-assembled film placed on an ethanol-filled cup. (b) Final assembly of modified Albert-Thwing cup. (c) Schematic of the test setup.

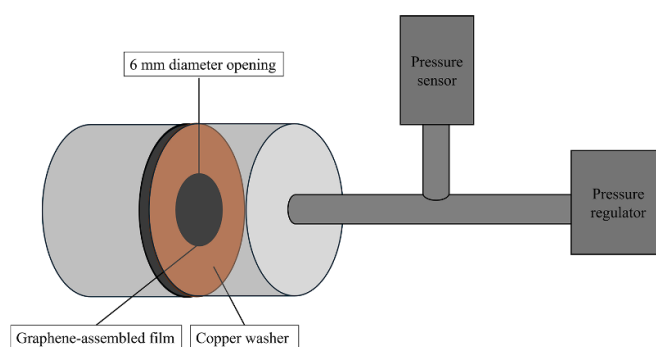


Figure 3. Illustration of test setup for burst-pressure testing of graphene-assembled film.

exposure to ethanol vapors. After conditioning, the THC was first measured on the fixture with the graphene-assembled film. Then the background concentration was measured by bypassing the fixture. A higher concentration on the sample compared to ambient air would indicate ethanol permeation through the graphene-assembled film.

Burst pressure was evaluated by clamping a graphene-assembled film in between a copper washer and a stainless-steel cylinder with a 6 mm in diameter orifice. The pressure was gradually increased with a manual Swagelok pressure regulator. A gauge pressure sensor with a measuring range between 0–2500 kPa was placed at the high-pressure side of the film. Graphene-assembled films with a thickness of 200 μm were burst pressure tested to evaluate if the film could withstand the maximum theoretical pressure levels in the vapor chambers during operation. A schematic of the test setup used for burst-pressure testing can be seen in figure 3.

Ethanol was the working fluid of choice in this study. It was chosen due to its superior wetting properties on graphene-assembled film compared to water. The good wettability of ethanol was evaluated by the sessile drop method and contact

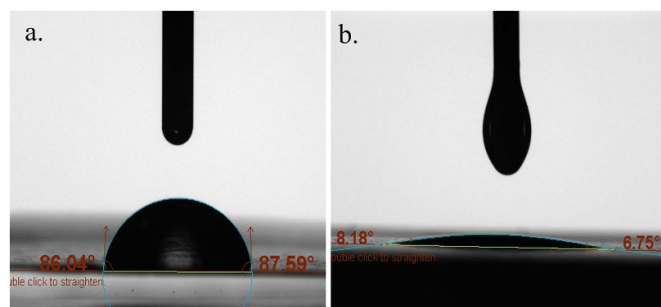


Figure 4. Wettability comparison between water and ethanol on graphene-assembled film. (a) Contact angle of water on graphene-assembled film. (b) Contact angle of ethanol on graphene-assembled film.

angle analysis with an optical tensiometer. The results can be seen in figure 4 which shows a contact angle comparison between water and ethanol on graphene-assembled film.

2.3. Vapor chamber design and fabrication

Graphene-assembled films with 100, 200 and 300 μm in thickness were used. The films were cut into square pieces with the dimension 56×56 mm. A copper mesh was bought from Goodfellow Cambridge Ltd to be used as a wick. The copper mesh had a nominal opening of 0.14 mm, a total thickness of 0.25 mm and a diameter of the copper thread of 0.115 mm. The open area of the mesh was 30.3% of the total area. Furthermore, copper spheres with a diameter of both 1 and 2 mm were bought from Goodfellow Cambridge Ltd to be used as spacers and structural support in the vapor chambers. The copper mesh was cut into 45×45 mm pieces and then soldered together in a sandwich structure with copper spheres in between two pieces of single layer copper mesh. The assembled mesh was placed in between two pieces of graphene-assembled film to act as a wick.

One vapor chamber design used solder as sealing material. A special solder with the trade name C-solder from Goodfellow Cambridge Ltd was used to solder the graphene-assembled films together. C-solder is specifically developed for soldering carbon-based materials. The perimeter of one graphene-assembled film was covered with a foil of C-solder and the copper mesh was placed in the center of the film. Another graphene-assembled film was placed on top, and the films were soldered together on a hot plate while applying pressure with an aluminum frame. The assembly procedure and the final assembled vapor chamber (VC 2) can be seen in figure 5.

As can be seen in figure 5, two nozzles were inserted into the vapor chambers, one for filling working fluid and the other for venting while filling. Three different vapor chambers were fabricated by using solder as sealing material. The vapor chambers were fabricated with different graphene-assembled film- and spacer thicknesses. The different configurations can be seen in table 1.

A vapor chamber with a different design was also fabricated by using a gasket instead of solder. In this design, a

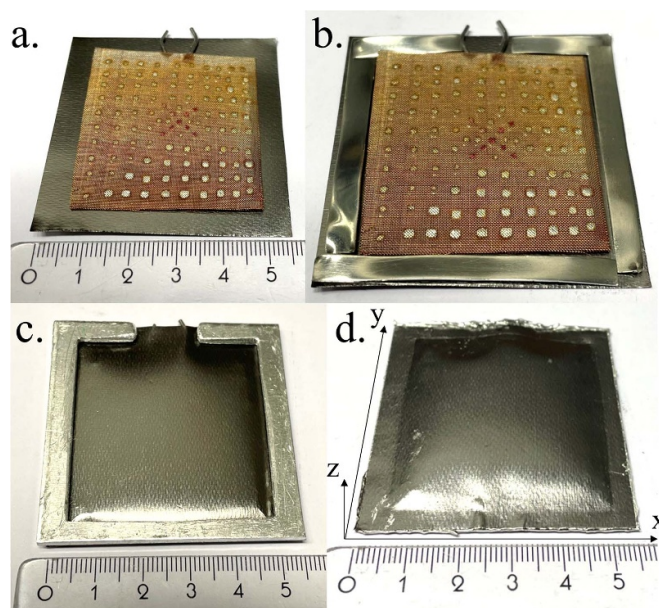


Figure 5. Fabrication steps of a soldered graphene-enhanced vapor chamber. (a) Copper mesh with 1 mm spacers on 200 μm graphene-assembled film. (b) C-solder is put on the perimeter of the graphene-assembled film before reflow. (c) A second graphene-assembled film was placed on top of the mesh and assembled with an aluminum frame during reflow. (d) The final graphene-enhanced vapor chamber.

Table 1. Three different graphene-enhanced vapor chamber design configurations were fabricated using the soldering method.

	Graphene-assembled film (μm)	Spacer diameter (mm)	Total VC thickness (mm)
VC 1	100	2.0	2.7
VC 2	200	1.0	1.9
VC 3	300	1.0	2.1

silicone-based thermal interface material with the tradename Compatherm from Nolato Silikonteknik AB was cut out and put on the perimeter of a 200 μm thick graphene-assembled film. Holes were drilled through the films and the silicone pad to be able to apply compression with ten M2 bolts around the perimeter. The vapor chamber was assembled with two 300 μm thick aluminum frames on each side for compression force distribution.

Figure 6 shows how the vapor chamber is assembled before it was filled with working fluid. The working fluid was supplied with a syringe through the opening that can be seen on the upper position of the vapor chamber in figure 6. The last step of the assembly process was to seal the opening by inserting a piece of silicone gasket and applying compression with a separate piece of aluminum.

A vapor chamber with a copper envelope was also fabricated by using the gasket sealing method. The envelope was made from 200 μm thick copper sheets. This was done to compare graphene-assembled film to copper as envelope material in a vapor chamber with the same design. All vapor chamber designs were characterized empty and with 0.5 ml ethanol

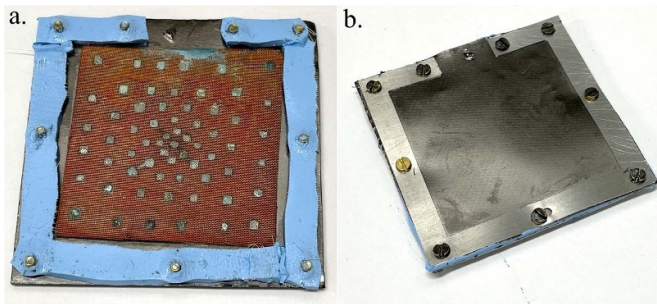


Figure 6. Assembly of a graphene-enhanced vapor chamber using a silicone thermal interface material as sealing gasket. (a) Copper mesh with 1 mm spacers on 200 μm graphene-assembled film with a silicone gasket on the perimeter. (b) Vapor chamber assembled with aluminum frames on both sides.

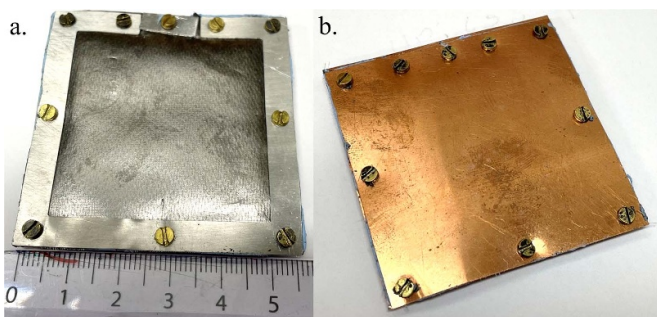


Figure 7. (a) Final assembly of a graphene-enhanced vapor chamber using the gasket sealing method. (b) Final assembly of a copper vapor chamber using the gasket sealing method.

to see how much the working fluid contributes to improved performance.

Figure 7 shows a graphene-enhanced vapor chamber and a copper vapor chamber after filling with ethanol and sealing with the gasket method.

2.4. Design and setup of thermal test rig

A thermal rig was designed to test the performance of the different vapor chamber configurations. The test rig was designed to simulate an 8×8 mm hot spot with the possibility to adjust the applied power density.

The hot spot was made from a 97 mm long copper bar with a 56×56 mm PEEK flange on top to distribute the clamping force evenly on the back side of the fairly flexible graphene-enhanced vapor chambers. The heat was generated by a cartridge heater that was inserted 75 mm into the copper bar. During measurements, the vapor chambers were clamped in between the hot spot and a water-cooled heat sink with an M10 bolt to be able to torque-control the mounting pressure.

The water-cooled heat sink was used to carry away the generated heat from the test rig. It was made from a 56×56 mm copper block with a milled cavity for water to flow through. The heat sink was customized to test the vapor chamber designs that were soldered. A small modification was necessary to characterize the vapor chambers with gasket sealing. To avoid direct contact between the assembly bolts and the heat

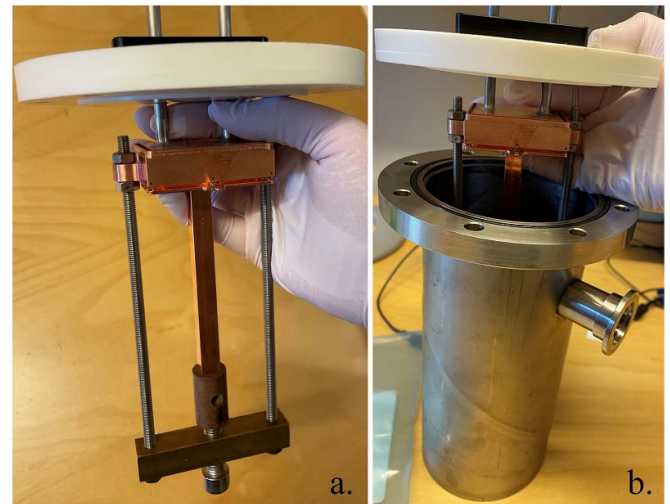


Figure 8. Customized thermal test rig for measuring thermal performance of vapor chambers and heat spreaders. (a) Heater and heat sink with a copper vapor chamber clamped in between. (b) Heater, heat sink and test specimen are placed in a steel container during measurements.

sink, a copper spacer with dimensions $40 \times 40 \times 5$ mm had to be put between the vapor chamber and the heat sink during characterization. A silicone-based thermal paste was applied between the copper spacer and the heat sink to decrease the contact resistance. A smaller PEEK flange with an area of 40×40 mm had to be used to apply the compression force during characterization. This test setup modification should be kept in mind when comparing results from the different vapor chamber designs to each other.

The whole characterization setup was operating inside a closed stainless-steel vessel to reduce the influence of convection losses on the measurements and thereby increase repeatability. The test fixture with the steel vessel is shown in figure 8.

The temperature measurements on the fixture were carried out with PT100 RTD sensors. There were two sensors in the heater bar, one was placed 4 mm from the cartridge heater, and another was placed 1 mm from the interface to the vapor chamber. There were three sensors in the heat sink block, measuring the temperature in two corners and in the center of the heat sink. The cooling-water temperature was measured with type-K thermocouples on the inlet and outlet. The temperature sensor configuration can be seen in figure 9.

The water-cooling system was driven by an Alphacool VPP655 pump and the flowrate was measured by a Gems TurboFlow FT-110 Series sensor. The cooling-water was pumped from an 8 l container and the outlet water was connected to a separate container to avoid a continuous temperature rise of the water during measurements.

2.5. Vapor chamber characterization

Power inputs of 30 and 50 W were used when characterizing the thermal performance of the vapor chambers. Higher power

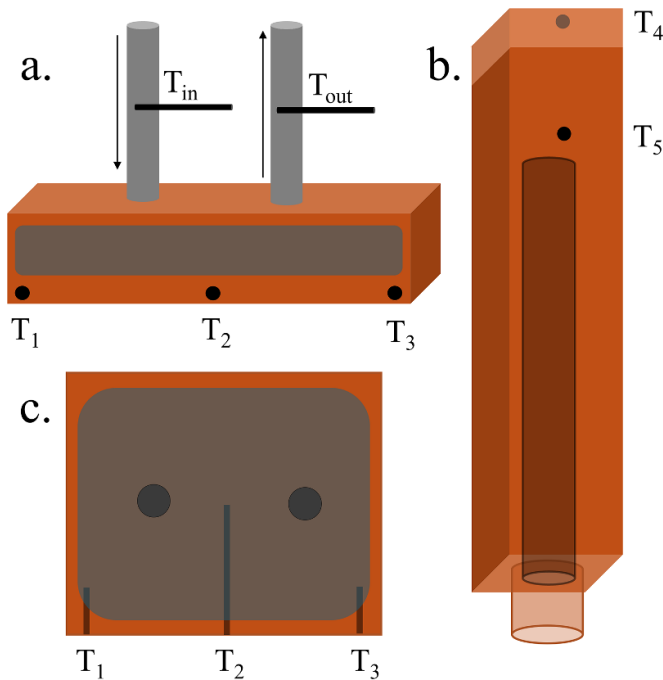


Figure 9. Outline of temperature sensors on the test setup. (a) Side view of the water-cooled heat sink. (b) Copper-bar with a reamed hole for a cartridge heater. (c) Top view of the water-cooled heat sink.

input than 50 W was not possible due to high hot spot temperatures for some vapor chamber designs. It is practical to avoid exceeding 100 °C from an electronics reliability perspective. Also, many modern CPUs have a maximum allowed junction temperature which is around 100 °C. Power inputs of 30 and 50 W correspond to a theoretical maximum power density of 47 and 78 W cm⁻² if convection and radiation losses from the heater to the air in the test chamber are neglected. However, since the comparison study was carried out in atmospheric pressure, heat losses can be expected to give a slightly lower power density than the theoretical maximum. The vapor chambers were clamped between the hot spot and heat sink with 0.4 Nm torque. A cooling-water flow rate of 1 ± 0.1 l min⁻¹ was used throughout all tests. All measurements were run for a minimum of 320 s. Before each measurement, the vapor chambers were filled with 0.5 ml of ethanol and sealed. The vapor chambers were weighed before and after thermal characterization to see if any working fluid was lost during operation.

The vapor chamber performance was evaluated by looking at the parameters, R_{Tot} and $R_{Tot, mass}$. To get a total thermal resistance of the vapor chambers it was necessary to account for the temperature difference in z -direction and in the x - y plane. Therefore, R_{Tot} was calculated by the following formula:

$$R_{Tot} = \frac{T_4 - \frac{T_1 + T_2 + T_3}{3}}{Q} \quad (1)$$

where T_1 , T_2 , T_3 , T_4 are the individual temperature readings in the test fixture and Q is the total power input. Furthermore,

to account for the mass of the device, $R_{Tot, mass}$ was calculated as a figure of merit.

$$R_{Tot, mass} = R_{Tot} * m_{VC} \quad (2)$$

where m_{VC} is the total mass of the operating vapor chamber.

3. Results and discussion

3.1. Permeability and burst pressure

A THC of 2.5 ± 0.5 ppm was measured after having conditioned the graphene-assembled film in ethanol vapors at 50 °C for 2 years and 4 months. The background hydrocarbon concentration in the air was also measured to be 2.5 ± 0.5 ppm. Thus, ethanol permeation through the graphene-assembled film could not be detected with the used conditioning time, temperature, film thickness and FID sensitivity. However, it could be possible that a longer conditioning time at higher temperature and with a thinner film would result in detectable ethanol permeation, this needs to be further studied.

Data from burst pressure tests on graphene-assembled films is presented in table 2. It can be seen that the burst pressure of a 200 μm thick graphene-assembled film ranges from 560 to >1040 kPa. The reason why sample 2 and 3 were not tested at higher pressures than 1040 kPa was due to limitations of the nitrogen gas supply system.

The vapor pressure of ethanol at 100 °C was estimated using the Antoine equation to be 226 kPa. This means that the burst pressure of graphene-assembled film is well above the theoretical maximum pressure of the vapor chambers in the temperature interval of the assessed application.

The permeability and burst pressure measurements were designed to evaluate the graphene-assembled film. However, the vapor chamber sealings are also a critical part of the design. In this study, the sealings were assessed by measuring mass loss of working fluid after thermal characterization. The different sealing methods can be further studied in more detail by performing permeability measurements and burst pressure tests.

3.2. Test method validation

Gasket sealed vapor chambers were characterized by five repetitive measurements in the thermal test rig. The vapor chambers were removed and put back in the test rig between every measurement. The total thermal resistance, R_{Tot} , was calculated after 330 s of each measurement.

Table 3 shows the total thermal resistance data from the characterization of a graphene-enhanced vapor chamber and a copper vapor chamber. The mean total thermal resistance of the graphene-enhanced vapor chamber was measured to 1.31 K W⁻¹ with a standard deviation of 0.02 K W⁻¹. The copper vapor chamber exhibited a mean thermal resistance of 1.72 K W⁻¹ with a standard deviation of 0.04 K W⁻¹. These results indicate good repeatability and validate the test method.

Table 2. Burst-pressure data for pristine 200 μm thick graphene-assembled films.

Sample	Burst pressure GF 200 (kPa gauge)
1	560
2	1040 ^a
3	>1040 ^b

^a Burst after 6 min.^b Did not burst for 28 min.**Table 3.** Measurements on a graphene-enhanced vapor chamber and a copper vapor chamber at 30 W power input to test the repeatability of the test method. The total thermal resistances are given for $t = 330$ s of the measurements.

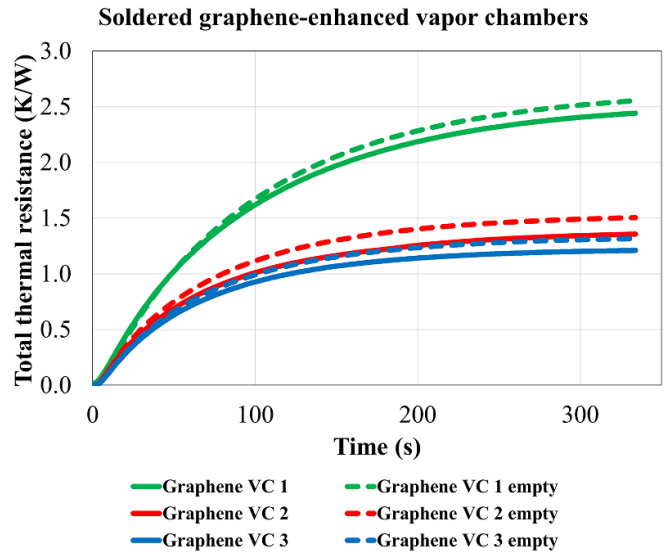
Test	Total thermal resistance GVC (K W^{-1})	Total thermal resistance CVC (K W^{-1})
1	1.32	1.72
2	1.32	1.78
3	1.35	1.72
4	1.30	1.67
5	1.29	1.69
Mean	1.31	1.72
Standard deviation	0.02	0.04

3.3. Vapor chamber characterization

The soldered graphene-enhanced vapor chambers were built with three different design configurations to evaluate the influence of graphene-assembled film thickness, spacer thickness and usage of working fluid on heat transfer.

Figure 10 shows a comparison of total thermal resistance R_{Tot} between the different graphene-enhanced vapor chamber designs outlined in table 1. It can be seen that VC 1 performs significantly worse compared to both VC 2 and VC 3. The difference is believed to be mainly due to the spacer thickness difference. The fact that VC 1 has a significantly higher thermal resistance than VC 2 and VC 3 indicates that the spacer diameter in the vapor chamber in this case is governing for the vapor chamber performance. It also implies that the air and ethanol vapor mixture in-between the two graphene-assembled films do not give the desired thermal conductivity between the evaporator and condenser. However, usage of working fluid is seen to have a positive effect on performance in all vapor chamber configurations, but the positive effect is lesser than what can be expected. A likely explanation for this is the existence of non-condensable gas which is encapsulated when the vapor chamber is sealed. Air inside the vapor chamber can cause a barrier for vapor transport to the condenser region [24]. It is known that the method used for vapor chamber assembly in this study allows entrapped non-condensable gas. It is also believed that the difference between an empty vapor chamber and one with working fluid would be more significant with an improved capillary performance of the wick.

Furthermore, figure 10 reveals that VC 3 performs best of the three vapor chambers. The only difference between VC 2

**Figure 10.** Total thermal resistance of soldered graphene-enhanced vapor chambers with different design configurations at 30 W power input.**Table 4.** Mass of soldered graphene-enhanced vapor chambers before and after characterization. 'Volume filled' is how much working fluid that the vapor chamber was initially filled with. 'Volume lost' is how much of the working fluid that had leaked during operation.

	Initial mass (g)	Mass after measurement (g)	Volume filled (ml)	Volume lost (ml)
VC 1	9.04	9.00	0.50	0.05
VC 2	10.41	10.19	0.50	0.28
VC 3	11.83	11.82	0.50	0.01

and VC 3 is that a thicker graphene-assembled film was used in VC 3. However, it cannot be concluded at this point that the difference is due to a thicker encapsulating material. It can possibly also be due to leak tightness of working fluid. If VC 2 lost more working fluid during operation than VC 3 then that can also be an explanation for worse performance.

The vapor chambers were weighed before and after characterization to see if any leakage occurred. The volume loss of working fluid during characterization was calculated based on mass loss. The results are summarized in table 4.

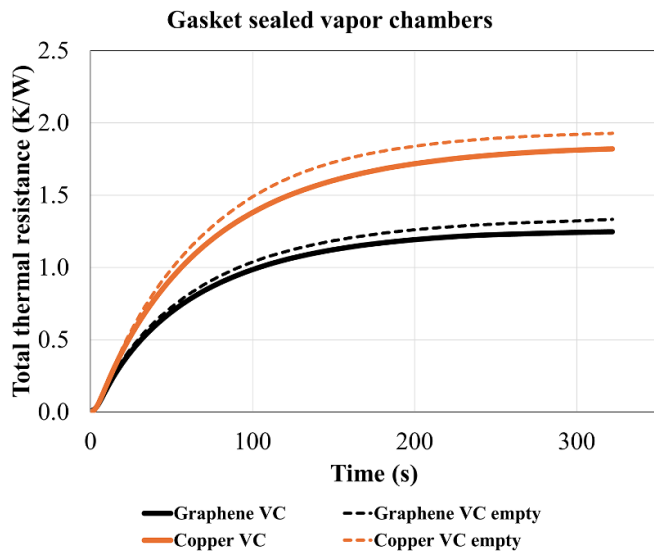
According to table 4, there is a difference in leak tightness between the vapor chambers. The difference in leak tightness can possibly explain why VC 3 performs better than VC 2.

It is also worth noticing that all measurements in figure 10 have not completely reached steady state after 320 s. The general trend is that vapor chambers with high thermal resistance do not reach steady state. Hence, the most likely explanation is that a fraction of the supplied energy is lost via convection and radiation to the test chamber and contributes to a continuous temperature increase of the system.

Table 5 shows that the gasket sealed vapor chambers demonstrate leak rates that are close to zero. Further studies

Table 5. Mass of gasket sealed graphene-enhanced vapor chamber and copper vapor chamber before and after characterization.

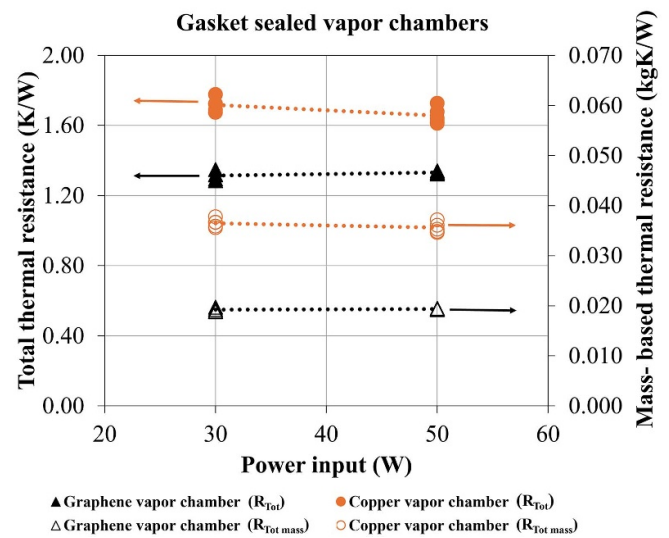
	Initial mass (g)	Mass after measurement (g)	Volume filled (ml)	Volume lost (ml)
Graphene VC	16.65	16.65	0.50	0.00
Copper VC	20.68	20.67	0.50	0.01

**Figure 11.** Total thermal resistance comparison of a graphene-enhanced vapor chamber and a copper vapor chamber at 30 W power input. The vapor chambers were built with a 200 μm thick envelope and were sealed with the gasket method.

would be required to determine with certainty if the mass loss is due to leakage, permeation through the gasket or evaporation of other volatiles from the gasket. Gasket sealing is, in contrast to soldering, a non-hermetic sealing method. Usage of non-hermetic sealings in a real application would result in working fluid permeation through the sealings over time. However, it was used in this study to evaluate the immediate effect of a better leak tightness of the built vapor chambers. More importantly, it was also used to show how graphene-assembled film can improve the performance of a vapor chamber in comparison to copper.

Figure 11 shows that the total thermal resistance in this single measurement is 0.57 K W^{-1} lower when graphene-assembled film is used as envelope instead of copper. The characterized vapor chambers were built with the same sealing technology and wick structure. Hence, this result suggests that using graphene-assembled film can be beneficial for effective heat dissipation in vapor chambers. Furthermore, table 5 shows that the graphene-enhanced vapor chamber weighs 4 grams less than the copper vapor chamber which is another argument for the benefits of graphene-assembled film.

Figures 10 and 11 also reveal that the total thermal resistance of the graphene-enhanced vapor chambers is similar regardless of sealing method. Furthermore, it is observed that the addition of working fluid lowers thermal resistance. These

**Figure 12.** Total thermal resistance and mass-based thermal resistance comparison of gasket sealed graphene and copper vapor chambers at different power inputs.

results imply that the superior leak tightness of the gasket sealed vapor chamber did not contribute to an evident effect on performance enhancement. Instead, it is believed that the existence of non-condensable gas and possibly poor capillary performance are the reasons for the relatively small performance gain of adding working fluid.

The gasket sealed vapor chambers were compared at both 30 and 50 W power input and the mass-based figure of merit, $R_{\text{Tot, mass}}$, was applied to showcase the benefit of the low density of graphene-assembled film. Each vapor chamber was characterized 5 consecutive times.

Figure 12 shows the thermal resistance and mass based thermal resistance at 30 and 50 W power input. The thermal resistance was calculated after 330 s measurement time. It can be seen that the measured thermal resistances are similar at 30 and 50 W power input for both tested vapor chambers. The mean thermal resistance of the graphene-enhanced vapor chamber is 21.6% lower than that of the copper vapor chamber in the tested power input interval. When comparing the mean mass-based thermal resistance, the graphene-enhanced vapor chamber is 46.5% better. It can also be seen that there is good repeatability of the measurements, especially for the graphene-enhanced vapor chamber. The standard deviation of the measured thermal resistance is slightly higher for the copper vapor chamber, a result that was also observed in the repeatability measurements shown in table 3. The higher standard deviation is possibly due to usage of thermal paste that adds extra uncertainty to the measurements.

From the results in this experimental study, it has been seen that graphene-assembled film can outperform copper as encapsulating material in vapor chambers. This result was observed when comparing vapor chambers that were built with the same method, working fluid and wick structure. However, some design changes are believed to be important to implement if the

graphene-enhanced vapor chambers should be able to compete with current commercial copper vapor chambers. The vapor chambers should be assembled with a method that evacuates non-condensable gas. It is also believed that the wick structure can be improved so that the capillary forces of the wick can transport the working fluid more efficiently. Furthermore, the vapor chambers made from graphene-assembled film in this study were limited to ethanol as working fluid. This is due to the poor wettability properties of water on graphene-assembled film. Improving hydrophilicity of the graphene-assembled film can possibly enable water as working fluid. This change could probably further improve performance, especially at higher power input since water has a higher enthalpy of vaporization and a higher boiling point compared to ethanol.

4. Conclusions

In this study, novel lightweight and high-performance graphene-enhanced vapor chambers were designed and built. The thermal performance of the vapor chambers was characterized in a customized test rig that simulates a hot spot. Different designs of the graphene-enhanced vapor chambers were fabricated using both solder and gasket sealing techniques. When characterized, the best thermal performance was observed when using 300 μm thick graphene-assembled film as envelope, 1 mm diameter copper spheres as spacers and 0.5 ml of ethanol as working fluid. With this design, the total thermal resistance was 1.21 K W^{-1} .

Thermal performance of a graphene-enhanced gasket sealed vapor chamber was compared to that of a copper vapor chamber with the same design. It was shown that using graphene-assembled film instead of copper as an envelope lowered thermal resistance of the vapor chamber by 21.6% and the mass-based thermal resistance by 46.5%.

Using graphene-assembled film instead of copper as an envelope can contribute to a lower thermal resistance of a vapor chamber. Hence, it is believed that graphene-enhanced vapor chambers can be built to surpass the performance of current commercial copper vapor chambers if state-of-the-art design guidelines and manufacturing standards are applied to remove non-condensable gas and optimize wick performance. If this is done, it is believed that the graphene-enhanced vapor chamber can replace conventional copper vapor chambers in future lightweight and high-performance cooling applications.

Data availability statement

The data that support the findings of this study are available upon reasonable request from the authors.


Acknowledgment

M Enmark and J Liu acknowledge the funding provided by 2D-TECH VINNNOVA competence center (Ref. 2019-00068). J Liu also acknowledges the financial support from

the Swedish National Science Foundation with the contract No: 621-2007-4660 and from the Production Area of Advance at Chalmers University of Technology. M Murugesan and H Zhang also acknowledge the support from Vinnova Siografen program. Finally, the authors would like to thank Lars Jönsson from the Department of Microtechnology and Nanoscience (MC2) at Chalmers University of Technology for his help with building the thermal test rig.

ORCID iDs

Markus Enmark  <https://orcid.org/0000-0001-6836-655X>

Arian Kamal  <https://orcid.org/0009-0004-3332-2097>

Johan Liu  <https://orcid.org/0000-0001-9931-1439>

References

- [1] Moore A L and Shi L 2014 Emerging challenges and materials for thermal management of electronics *Mater. Today* **17** 163–74
- [2] Chen X, Ye H, Fan X, Ren T and Zhang G 2016 A review of small heat pipes for electronics *Appl. Therm. Eng.* **96** 1–17
- [3] Bulut M, Kandlikar S G and Sozbir N 2019 A review of vapor chambers *Heat Transf. Eng.* **40** 1551–73
- [4] Ganvir R B, Walke P V and Kriplani V M 2017 Heat transfer characteristics in nanofluid-A review *Renew. Sustain. Energy Rev.* **75** 451–60
- [5] Tsai C Y, Chien H T, Ding P P, Chan B, Luh T Y and Chen P H 2004 Effect of structural character of gold nanoparticles in nanofluid on heat pipe thermal performance *Mater. Lett.* **58** 1461–5
- [6] Kang S-W, Wei W-C, Tsai S-H and Yang S-Y 2006 Experimental investigation of silver nano-fluid on heat pipe thermal performance *Appl. Therm. Eng.* **26** 2377–82
- [7] Alhuyi Nazari M, Ghasempour R, Hossein Ahmadi M, Heydarian G and Behshad Shafii M 2018 Experimental investigation of graphene oxide nanofluid on heat transfer enhancement of pulsating heat pipe *Int. Commun. Heat Mass Transf.* **91** 90–94
- [8] Putra N, Septiadi W N, Sahnura R and Anggara C T 2013 Application of Al_2O_3 nanofluid on sintered copper-powder vapor chamber for electronic cooling *Adv. Mater. Res.* **789** 423–8
- [9] Vadakkan U, Chrysler G M, Maveety J and Tirumala M 2007 A novel carbon nano tube based wick structure for heat pipes/vapor chambers *Twenty-Third Annu. IEEE Semicond. Therm. Meas. Manag. Symp.* pp 102–4
- [10] Cai Q and Chen C L 2010 Design and test of carbon nanotube biwick structure for high-heat-flux phase change heat transfer *J. Heat Transf.* **132** 1–8
- [11] Weibel J A, Garimella S V, Murthy J Y and Altman D H 2011 Design of integrated nanostructured wicks for high-performance vapor chambers *IEEE Trans. Compon. Packag. Manuf. Technol.* **1** 859–67
- [12] Solomon A B, Ramachandran K and Pillai B C 2012 Thermal performance of a heat pipe with nanoparticles coated wick *Appl. Therm. Eng.* **36** 106–12
- [13] Nam Y, Sharratt S, Byon C, Kim S J and Ju Y S 2010 Fabrication and characterization of the capillary performance of superhydrophilic Cu micropost arrays *J. Microelectromechanical Syst.* **19** 581–8
- [14] Moss A, Antoniou A and Smet V 2023 High performance, multilayer copper-graphene micro-foam wicks for vapor

- chambers 2023 *IEEE 73rd Electron. Components Technol. Conf.* pp 2087–92
- [15] Liu Y, Chen S, Fu Y, Wang N, Mencarelli D, Pierantoni L, Lu H and Liu J 2021 A lightweight and high thermal performance graphene heat pipe *Nano Sel.* **2** 364–72
- [16] Alvarado S, Maldonado P and Jaques I 1999 Energy and environmental implications of copper production *Energy* **24** 307–16
- [17] Wang N *et al* 2018 Tailoring the thermal and mechanical properties of graphene film by structural engineering *Small* **14** 1801346
- [18] Torres F G, Troncoso O P, Rodriguez L and De-La-Torre G E 2021 Sustainable synthesis, reduction and applications of graphene obtained from renewable resources *Sustain. Mater. Technol.* **29** e00310
- [19] Chen J, Yao B, Li C and Shi G 2013 An improved Hummers method for eco-friendly synthesis of graphene oxide *Carbon* **64** 225–9
- [20] Chen S, Wang Q, Zhang M, Huang R, Huang Y, Tang J and Liu J 2020 Scalable production of thick graphene films for next generation thermal management applications *Carbon* **167** 270–7
- [21] Guo S *et al* 2022 Toward ultrahigh thermal conductivity graphene films *2D Mater* **10** 14002
- [22] Kallio K and Hedenqvist M 2010 Test method effects of ethanol content and temperature on the permeation of fuel through polyamide-12-based pipes *Polym. Test.* **29** 603–8
- [23] Scanlon J T and Willis D E 1985 Calculation of flame ionization detector relative response factors using the effective carbon number concept *J. Chromatogr. Sci.* **23** 333–40
- [24] Bérut E, Lips S, Lefèvre F and Sartre V 2021 Effect of non-condensable gas on heat transfer within the hollow fin condenser of metallic and polymer vapor chambers *Appl. Therm. Eng.* **190** 1359–4311